Genome-wide CRISPR activation screen identifies novel receptors for SARS-CoV-2 entry

Shiyou Zhu[1,*], Ying Liu[1,*], Zhuo Zhou[1,*], Zhiying Zhang[2,*], Xia Xiao[3], Zhiheng Liu[1], Ang Chen[1,4], Xiaojing Dong[3], Feng Tian[1], Shihua Chen[2,4], Yiyuan Xu[1], Chunhui Wang[1], Qiheng Li[1], Xuran Niu[1], Qian Pan[1], Shuo Du[2], Junyu Xiao[2,†], Jianwei Wang[3,†], Wensheng Wei[1,†]

[1]Biomedical Pioneering Innovation Center, Beijing Advanced Innovation Center for Genomics, Peking-Tsinghua Center for Life Sciences, Peking University Genome Editing Research Center, State Key Laboratory of Protein and Plant Gene Research, School of Life Sciences, Peking University, Beijing 100871, China.

[2]State Key Laboratory of Protein and Plant Gene Research, School of Life Sciences, Peking University, Beijing, China; Peking-Tsinghua Center for Life Sciences, Peking University, Beijing, China; Beijing Advanced Innovation Center for Genomics, Peking University, Beijing 100871, China.

[3]NHC Key Laboratory of Systems Biology of Pathogens and Christophe Mérieux Laboratory, Institute of Pathogen Biology, Chinese Academy of Medical Sciences and Peking Union Medical College, Beijing 100730, China; Key Laboratory of Respiratory Disease Pathogenomics, Chinese Academy of Medical Sciences and Peking Union Medical College, Beijing 100730, China.

[4]Academy for Advanced Interdisciplinary Studies, Peking University, Beijing 100871, China.

*These authors contributed equally to this work.

†Correspondence: junyuxiao@pku.edu.cn (J.X.), wangjw28@163.com (J.W.) and wswei@pku.edu.cn (W.W.)

The ongoing pandemic of coronavirus disease 2019 (COVID-19) caused by severe acute respiratory syndrome coronavirus 2 (SARS-CoV-2) has been endangering worldwide public health and economy. SARS-CoV-2 infects a variety of tissues where the known receptor ACE2 is low or almost absent, suggesting the existence of alternative pathways for virus entry. Here, we performed a genome-wide barcoded-CRISPRa screen to identify novel host factors that enable SARS-CoV-2 infection. In addition to known host proteins, i.e. ACE2, TMPRSS2 and NRP1, we identified multiple host components, among which LDLRAD3, TMEM30A and CLEC4G were confirmed as functional receptors for SARS-CoV-2. All these membrane proteins bind directly to spike's N-terminal domain (NTD). Their essential and physiological roles have all been confirmed in either neuron or liver cells. In particular, LDLRAD3 and CLEC4G mediate SARS-CoV-2 entry and infection in a fashion independent of ACE2. The identification of the novel receptors and entry mechanisms could advance our understanding of the multiorgan tropism of SARS-CoV-2, and may shed light on the development of the therapeutic countermeasures against COVID-19.

The outbreak of coronavirus disease 2019 (COVID-19) has caused a global health crisis. The etiologic agent of COVID-19 is acute respiratory syndrome coronavirus 2 (SARS-CoV-2), a positive-stranded betacoronavirus (*1, 2*). SARS-CoV-2 is the seventh coronavirus known to infect humans, and is the third coronavirus, after severe acute respiratory syndrome (SARS)-CoV and Middle East respiratory syndrome (MERS)-CoV, that has caused outbreaks with significant fatality rates (*3*). SARS-CoV-2 mainly infects the respiratory system, causing symptoms at the onset of disease as fever, cough, fatigue, and myalgia (*4, 5*). Moreover, COVID-19 is associated with high rates of multiorgan symptoms, such as neurological (*6*), renal (*7*), gastrointestinal (*8*), and cardiovascular (*9*) complications, indicating the broad organotropism of SARS-CoV-2.

Like SARS-CoV, SARS-CoV-2 engages human angiotensin-converting enzyme 2 (ACE2) as the receptor to enter host cells (*10*). The interaction between SARS-CoV-2 and ACE2 is mediated by the receptor-binding domain (RBD) of the SARS-CoV-2 spike (S) glycoprotein. Following binding to ACE2, S protein is cleaved into S1 and S2 domains by cellular proteases such as furin, followed by further cleavage of S2 by proteases such as TMPRSS2 or cathepsins (*11, 12*). This "priming" process triggers dramatic conformational changes of the S2 domain to enable the fusion of the viral envelope with cellular membranes, thereby allowing the release of the viral genome into host cells (*11,*

55 *13*). Despite data showing that ACE2 is a high-affinity receptor for SARS-CoV-2 (*14*), lines of evidence
56 suggested that alternative receptors or pathways may exist. First, the tissue distribution pattern of ACE2
57 does not fully correlate with SARS-CoV-2 tropism, questioning the ACE2-dependent pathway as the
58 sole entry route. Analyses of the single-cell RNA sequencing data indicated that ACE2 is expressed low
59 throughout the respiratory tract, the primary infection site of SARS-CoV-2 (*15, 16*). Moreover, SARS-
60 CoV-2 infects the brain, and viral RNA has been detected in immune cells such as neutrophils,
61 macrophages, T/B cells, and NK cells (*17, 18*), whereas ACE2 is barely detected in these tissues or cells
62 (fig. S1). Second, a recent report showed that an ACE2-null lung adenocarcinoma cell is highly
63 permissive to SARS-CoV-2 (*19*), indicating that SARS-CoV-2 could leverage an alternative receptor for
64 its entry. Third, a cell surface protein, AXL, has recently been reported to facilitate SARS-CoV-2 entry
65 independently of ACE2 (*20*). NRP1 was found to function as an ACE2-dependent host factor, which is
66 highly expressed in human pulmonary and olfactory neuronal cells of the epithelium, and could bind to
67 S1 CendR motif of the viral spike protein (*21, 22*). Altogether, it is plausible to postulate that SARS-
68 CoV-2 may gain its entry to host cells via alternative receptor(s) other than ACE2.
69
70 Functional genomics approaches such as CRISPR knockout screens have been conducted to search for
71 critical host factors involved in SARS-CoV-2 infection (*23-26*). However, none of these screens could
72 pinpoint novel receptors beyond ACE2, possibly due to the fact that such loss-of-function screens were
73 performed based on cell types that the expression and function of ACE2 are dominant. Herein, aiming to
74 systematically interrogate host factors for SARS-CoV-2 entry, we performed a genome-wide CRISPR
75 activation screen in HEK293T cells using the SARS-CoV-2 spike-pseudotyped virus (*27*). Such gain-of-
76 function screen could potentially identify those proteins that confer host cell susceptibility to SARS-
77 CoV-2.
78
79 To establish a CRISPRa screening for the identification of viral entry factors, we utilized pseudotyped
80 virus harboring the SARS-CoV-2 spike protein and an EGFP marker that indicates viral infection. EGFP
81 signal was barely detectable two days after infection with different amounts of SARS-CoV-2
82 pseudovirus in HEK293T cells, unlike infection by lentivirus harboring the vesicular stomatitis virus G
83 protein (VSV-G) (fig. S2A), indicating that SARS-CoV-2 pseudovirus hardly infects HEK293T cells.
84 This was likely due to the lack of sufficient expression of functional receptors in HEK293T cells.
85 Indeed, HEK293 cells stably overexpressing ACE2 were highly susceptible to SARS-CoV-2

86 pseudovirus, and the EGFP signal was proportionally boosted with the increase of pseudovirus (fig.
87 S2B). We then tested the effect of gene activation through CRISPRa using the 50-fold concentrated
88 pseudovirus. In HEK293T cells stably expressing CRISPRa system (HEK293T-CRISPRa cells), the
89 upregulation of *ACE2* by sgRNA1^{ACE2} and sgRNA5^{ACE2} enabled the infection of SARS-CoV-2
90 pseudovirus with a significant boost of EGFP expression within the cells (Fig. 1A). As such, we
91 developed a CRISPRa screen method to identify host factors enabling SARS-CoV-2 infection.
92
93 To reach the optimal performance using the CRISPR activation system (*28*), we tended to construct a
94 genome-wide CRISPRa library with all sgRNAs barcoded so that we could benefit from a high
95 multiplicity of infection (MOI) in generating the cell library, an approach we previously established
96 (*29*). Because the loops of sgRNAs are used for such a CRISPRa system we employed (*28*), we decided
97 to add the barcodes at the external region outside of sgRNA at its 3' end, designated as eBAR, instead of
98 iBAR we designed before (*29*). Three external barcodes of 4-nt were assigned to each sgRNA (Fig. 1B).
99 The oligos of sgRNA library (*30*) were synthesized and respectively cloned into three lentiviral
100 sgRNA^{eBAR} backbones (table S1). The sgRNA^{eBAR} library was delivered into HEK293T-CRISPRa cells
101 by lentiviral infection at an MOI of ~10. The pseudovirus (50-fold) was added to the library cells, and
102 the infected cells were sorted by FACS (fig. S3A). Since the EGFP signal was maintained in the sorted
103 cells and could not completely fade out, we were not able to perform multiple rounds of enrichment to
104 reduce noises (Fig. 1E-H). We therefore categorized screening results based on fluorescence intensity,
105 and selected those top candidates from each group to maximize the chance of target identification. After
106 two rounds of pseudovirus infection and sorting, we collected total EGFP^{+} cells as well as top 10-20%,
107 top 10% and top 2% of sorted cells grouped by the EGFP intensity (Fig. 1C-D and fig. S3B). We
108 generated screen scores for genes in each EGFP^{+} group considering the performance of all their
109 targeting sgRNAs^{eBAR} (Fig. 1E-H, table S2, see Methods). In most groups, the known SARS-CoV-2
110 receptor ACE2 (*11, 13, 31*) and the main host protease TMPRSS2 (*11*) were significantly enriched. We
111 also identified other reported host factors for SARS-CoV-2 entry, such as NRP1 (*21, 22*). The EGFP
112 intensity was supposed to represent the strength of the target host factor in promoting virus entry. Thus
113 we assumed that receptors were more likely to be identified from groups with higher EGFP intensity.
114 For example, ACE2 was ranked higher in the top 2% than in other groups (Fig. 1E-H).
115

116 To further characterize these identified host factors, we performed Gene Ontology (GO) enrichment
117 analysis (*32*). A number of genes were enriched in multiple important cellular processes, such as
118 regulation of plasma membrane-bound cell projection organization, vesicle-mediated transport, receptor-
119 mediated endocytosis, and viral life cycle (Fig. 2A, fig. S4, table S3). Many of these genes were top-
120 ranked in most groups of the sorted $EGFP^{+}$ cells (Fig. 2B). Assuming that the intensity of EGFP
121 represented the strength of candidate factors in facilitating virus entry, we were particularly interested in
122 membrane proteins identified from the top 2% and 10% groups. For other types of candidates, we
123 pooled top-ranked candidates in all four groups for validation. For each gene, we found that most of its
124 corresponding $sgRNAs^{eBAR}$ were significantly enriched, indicating the reliability of our selection on the
125 top hits. Besides, most of the functional sgRNAs performed consistently with their eBARs (fig. S5). The
126 gene expression analysis revealed that several genes are widely expressed in multiple tissues such as
127 *TMEM30A* and *CTSL*, and some genes' expressions are more tissue-specific, such as brain-specific
128 genes *CPLX1*, *LDLRAD3*, *GPM6B* and *EPHB1*, liver-specific genes *CLEC4G* and *MASP1*, lung-
129 specific genes *CLEC5A* and *HLA-DQA1*, and immune-specific genes *ICAM2* and *STAMBPL1* (Fig. 2C).
130 These findings hold the potential to interpret the organotropism of SARS-CoV-2 especially where the
131 known receptors and other entry factors were lowly expressed.
132
133 To validate the candidate genes identified from our screen, we focused particularly on membrane
134 proteins, proteases, and some other top-ranked hits. For a total of 51 candidates, we transduced
135 HEK293T cells with their corresponding cDNAs, followed by infection with SARS-CoV-2 pseudotyped
136 virus containing a luciferase reporter (*27*). As the known receptor or co-receptor for SARS-CoV-2, the
137 ectopic expression of ACE2 or NRP1 greatly promoted the pseudotyped virus infection (Fig. 3A). A
138 number of novel host factors have been confirmed to facilitate SARS-CoV-2 pseudovirus entry,
139 including some membrane proteins, LDLRAD3, TMEM30A, CLEC4G, CPLX1, and CA9 (Fig. 3A).
140 LDLRAD3 is a member of the LDL scavenger-receptor family that is highly expressed in neurons and
141 has been reported to regulate amyloid precursor protein in neurons (*33*). TMEM30A is a transmembrane
142 protein involved in membrane trafficking and signaling pathways as a heterocomplex with ATP8A1 by
143 regulating the translocation of phospholipids (*34*). CLEC4G is a member of the C-type lectin family that
144 has been reported to enhance the infection of SARS-CoV by interacting with its spike protein (*35*).
145 CPLX1 is a member of the complexin/synaphin family involved in synaptic vesicle exocytosis and
146 transmitter release (*36*). CA9, a transmembrane protein and a tumour marker (*37*), has also been reported

147 to be involved in HBV infection (*38*). Interestingly, two proteases, STAMBPL1 and TMPRSS15, were
148 also identified with their confirmed roles to promote SARS-CoV-2 pseudovirus infection (Fig. 3A).
149 Proteases such as TMPRSS2 are known to play critical roles in ACE2-dependent virus entry (*11*).
150 Therefore, we reasoned that proteases with similar functions could promote virus entry upon
151 overexpression. We went on to validate these candidate genes using the authentic SARS-CoV-2 virus. In
152 HEK293T cells, besides *ACE2* and *CTSL*, the ectopic expression of any of the following genes could
153 effectively enable SARS-CoV-2 infection, *CLEC4G*, *CPLX1*, *LDLRAD3*, *TMEM30A*, and *STAMBPL1*
154 (Fig. 3B).
155
156 To examine if ACE2 is required for any of these candidate components to promote viral infection, we
157 generated HEK293T *ACE2*$^{-/-}$ cells (fig. S6). We found that the function of CA9, CLEC4G, and
158 LDLRAD3 in facilitating luciferase reporter pseudovirus infection is independent of ACE2 (Fig. 3C). In
159 the test of authentic virus infection, overexpression of either CLEC4G or LDLRAD3 is sufficient to
160 enable SARS-CoV-2 infection in HEK293T *ACE2*$^{-/-}$ cells (Fig. 3D).
161
162 Next, we focused on characterizing these membrane proteins and evaluating whether any of them serves
163 as a functional receptor for SARS-CoV-2. We first examined whether there are interactions between
164 these receptor candidates and SARS-CoV-2 spike (S) protein. Co-immunoprecipitation (Co-IP) assay
165 showed that SARS-CoV-2 S co-precipitated with multiple candidate proteins including TMEM30A,
166 ICAM2, CA9, LDLRAD3, CLEC4G, and the known host factors, ACE2, NRP1, TMPRSS2 and CTSL,
167 but not with STAMBPL1 and CPLX1 (Fig. 4A). We then purified these proteins (fig. S7A) to examine
168 the direct interactions by the pull-down assay. Like ACE2, LDLRAD3 and CLEC4G efficiently pulled
169 down SARS-CoV-2 S (Fig. 4B). Reciprocally, SARS-CoV-2 S pulled down LDLRAD3, CLEC4G and
170 ACE2, but not CA9 (fig. S7B). Moreover, we determined domains on SARS-CoV-2 S that mediate the
171 interactions. In consistent with previous reports (*10*), ACE2 interacted with RBD but not NTD (Fig. 4D
172 and 4C). However, NTD but not RBD were found to directly interact with LDLRAD3, CLEC4G, and
173 TMEM30A (Fig. 4C-D).
174
175 In light of these direct binding results, we predicted that the extracellular addition of these purified
176 proteins could prevent virus entry by competing cellular receptors for binding to S. To test this idea, we
177 incubated serially diluted soluble proteins with authentic SARS-CoV-2 virus before infection. The

178 addition of soluble ACE2 (Fig. 5A and 5B) and LDLRAD3 (Fig. 5C and 5D) were capable of protecting
179 both SH-SY5Y (Fig. 5A and 5C) and SK-N-SH (Fig. 5B and 5D), two neuroblastoma cell lines, from
180 SARS-CoV-2 infection, in a dose-dependent manner. Similarly, the addition of soluble ACE2 (Fig. 5E)
181 and CLEC4G (Fig. 5F) effectively suppressed SARS-CoV-2 infection in a liver cancer cell line Huh7.5,
182 also in a dose-dependent manner.
183
184 SARS-CoV-2's entry is initiated by the interaction between the spike and its host receptor(s), followed
185 by furin-mediated cleavage at the S1/S2 site and the priming via TMPRSS2 or other surface/endosomal
186 proteases (*39, 40*). The surface subunit S1 of spike is responsible for binding to the host receptor, and
187 the transmembrane subunit S2 mediates the viral and cellular membrane fusion (*11*). Previous studies
188 have shown that SARS-CoV-2 S present in the plasma membrane possesses high fusogenic activity and
189 could trigger receptor-dependent fusion with neighboring cells, leading to the formation of
190 multinucleated giant cells (syncytia) (*40, 41*). To examine whether the interaction between the SARS-
191 CoV-2 spike protein and our newly identified receptors could elicit membrane fusion, we performed a
192 co-culture assay to determine the syncytium formation. The wild-type HEK293T cells transfected with
193 plasmids expressing S and EGFP were mixed with HEK293T cells stably overexpressing individual
194 candidate receptors labelled with an mCherry marker (see Methods). At 40 h post cell co-culture, cells
195 expressing any of the following, *ACE2*, *CLEC4G*, *LDLRAD3* and *TMEM30A*, substantially fused with
196 cells expressing S, manifested by the colocalization of the EGFP and mCherry fluorescent signals in the
197 merged images, which could be visualized even in the bright field (Fig. 6). In comparison, the control
198 cells infected with only the empty vector showed no syncytium formation, nor merged fluorescent
199 signals (Fig. 6). These observations suggested that any of CLEC4G, LDLRAD3 and TMEM30A
200 functionally interacts with spike protein of SARS-CoV-2 S to trigger membrane-to-membrane fusion, a
201 critical step for receptor-mediated viral entry, just as ACE2.
202
203 To evaluate their physiological roles, we first conducted expression analysis using the Human Protein
204 Atlas (HPA) (*42*). LDLRAD3 is preferentially expressed in brain tissue, such as cerebellum, spinal cord
205 and salivary gland (fig. S8A). The expression of CLEC4G could only be detected in liver and lymph
206 node (fig. S8B). While TMEM30A is more ubiquitously expressed in tissues including those with a high
207 incidence of infection, such as lung, colon and airway (fig. S8C). We then tested whether these
208 candidate receptors are required for SARS-CoV-2 in specific cells. *TMEM30A* and *LDLRAD3* showed

209 much higher expression compared to *ACE2* in SH-SY5Y cells, which is consistent with the analysis
210 from HPA (Fig. 7A). The siRNAs targeting *ACE2*, *TMEM30A*, *LDLRAD3* were introduced into
211 indicated cells followed by authentic SARS-CoV-2 infection (table S4). Efficient knockdown was
212 confirmed by qPCR analysis (Fig. 7B-D). The disruption of *ACE2*, *LDLRAD3* and *TMEM30A*
213 expression all led to significant cellular resistance to SARS-CoV-2 infection (Fig. 7E). Of note, the
214 extent of siRNA knockdown correlated well with the inhibitory effects to the viral infection (Fig. 7E).
215 Similar in SH-SY5Y, *LDLRAD3* and *TMEM30A* were highly expressed in another neuron cell line, SK-
216 N-SH (Fig. 7F). Moreover, the expression of *ACE2* in SK-N-SH was too low to be detected through
217 qPCR. The siRNA knockdown of *LDLRAD3* and *TMEM30A* (Fig. 7G and H) significantly blocked
218 SARS-CoV-2 infection, whereas *ACE2*-targeting siRNAs exerted no effects, likely due to the lack of
219 endogenous *ACE2* expression (Fig. 7I). As CLEC4G is preferentially expressed in the liver, we tested its
220 function in Huh7.5 cells. The qPCR results indicated a lower expression level of *CLEC4G* than *ACE2* in
221 Huh7.5 (Fig. 7J). Nevertheless, knockdown of either *ACE2* or *CLEC4G* (Fig. 7K and L) significantly
222 inhibited SARS-CoV-2 infection in Huh7.5 cells (Fig. 7M). These results clearly demonstrated the
223 essential roles of LDLRAD3, TMEM30A and CLEC4G in SARS-CoV-2 infection, especially in cell
224 types where ACE2 was lowly expressed.
225
226 Here we conducted a study of applying a gain-of-function screen for SARS-CoV-2 entry, which
227 uncovered three new viral receptors besides ACE2. Of the candidate receptors identified in this study,
228 LDLRAD3 is highly expressed in neurons, and its overexpression robustly enhanced SARS-CoV-2
229 infection in both wild-type and HEK293T *ACE2*$^{-/-}$ cells. LDLRAD3 has recently received attention as a
230 critical receptor for the Venezuelan equine encephalitis virus (VEEV) (*43*). Similar to VEEV, SARS-
231 CoV-2 was also reported to infect the brain (*7*). Our data revealed that knockdown of LDLRAD3 or
232 supplement of its soluble protein could dramatically reduce SARS-CoV-2 infection in neuron cells,
233 suggesting its critical function in mediating viral entry in neurons. Moreover, another confirmed ACE2-
234 independent candidate receptor, CLEC4G, was known to be highly expressed in the liver (*44*), lymph
235 node and monocytes (fig. S8B). This gene encodes a glycan-binding receptor and is a member of the C-
236 type lectin family, which has been found to facilitate SARS-CoV attachment through glycan-binding
237 (*35*). Herein, we demonstrated for the first time CLEC4G's role in SARS-CoV-2 entry. Interestingly, the
238 transmembrane protein TMEM30A was also identified in a recent genome-wide knockout screen for
239 SARS-CoV-2 in Huh7.5 cells (*23*). Our study confirmed its essentiality for SARS-CoV-2 entry and its

direct binding with SARS-CoV-2 S. The discovery of multiple receptors in this study, with either tissue-specific or broad-spectrum expression patterns, might provide clues for understanding the multiorgan tropism of SARS-CoV-2 (*7*).

It's worth noting that all these receptors we identified bind to the NTD domain of S, rather than RBD, the ACE2-binding domain, suggesting that NTD of SARS-CoV-2 S also plays important roles in mediating virus entry. Recent reports showed that NTD-specific neutralization antibodies isolated from convalescent COVID-19 patients enabled robust protection from the SARS-CoV-2 challenge (*45, 46*). It is possible that NTD-targeting antibodies might function by blocking NTD mediated virus entry.

Besides membrane proteins, we have also discovered several proteases, i.e., STAMBPL1 and TMPRSS15, whose overexpression promoted SARS-CoV-2 infection. The synergy of receptors and proteases in different tissues is worth of further investigation. Finally, the novel identified receptors or other functional factors brought a more comprehensive understanding for SARS-CoV-2 infection and might serve as novel therapeutic targets for COVID-19.

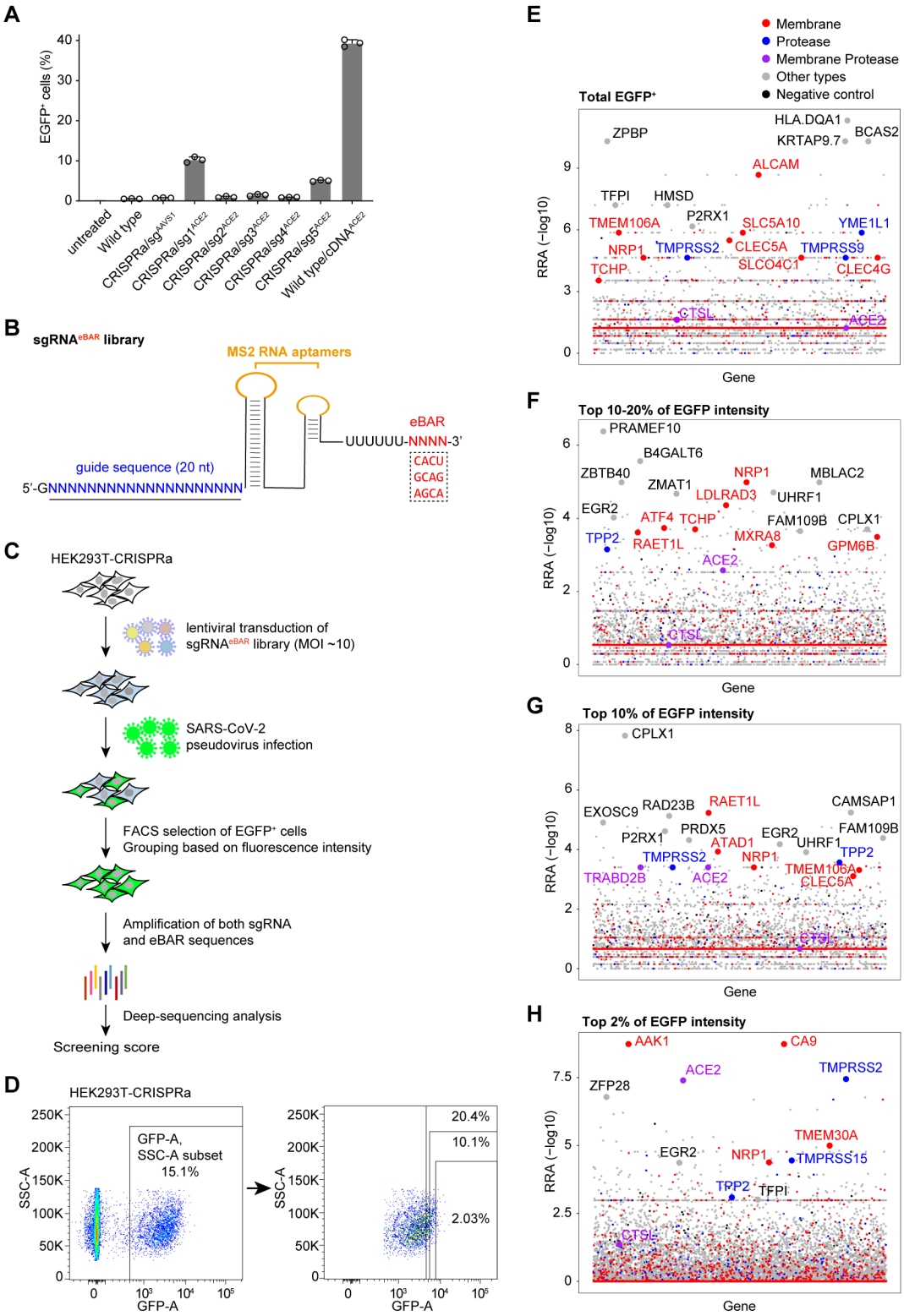

Fig. 1. Identification of candidate factors for SARS-CoV-2 entry by a genome-wide CRISPRa gain-of-function screen in HEK293T cells. (**A**) Detection of the pseudovirus infection in HEK293T-

262 CRISPRa cells transfected with different sgRNAs targeting *ACE2*. The infection rate of SARS-CoV-2
263 pseudovirus is indicated by the percentage of EGFP positive cells. Wide type/cDNA^{ACE2} represents the
264 wild type HEK293T cells transfected with ACE2 cDNA as a positive control. (**B**) Schematic diagram of
265 an sgRNA with an external barcode (eBAR). Three 4-nt eBARs were respectively embedded outside of
266 the sgRNA scaffold after the poly-U signal. (**C**) Schematic of the CRISPRa screen in HEK293T cells
267 using the SARS-CoV-2 pseudotyped virus. (**D**) FACS selection of EGFP^{+} cells grouping based on
268 different fluorescence intensities after SARS-CoV-2 pseudovirus infection. Left indicates the total EGFP
269 intensity of HEK293T-CRISPRa library cells after second round of pseudovirus infection. Right
270 indicates three additional sorting gates including top 10-20%, top 10% and top 2% of the total EGFP^{+}
271 cells. (**E**-**H**) Robust rank aggregation (RRA) scores of all genes from the total EGFP^{+} (**E**), top 10-20%
272 (**F**), top 10% (**G**) and top 2% (H) of the total EGFP^{+} cells. RRA scores were used to evaluate the
273 enrichment of candidate genes, which were calculated by binomial *p*-values of sgRNAs^{eBAR} targeting
274 each gene. Membrane proteins were labelled as red dots, proteases were labelled as blue dots, the genes
275 that are both membrane protein and proteases were labelled as purple dots. Grey and black dots
276 represent other types of genes and negative controls.
277

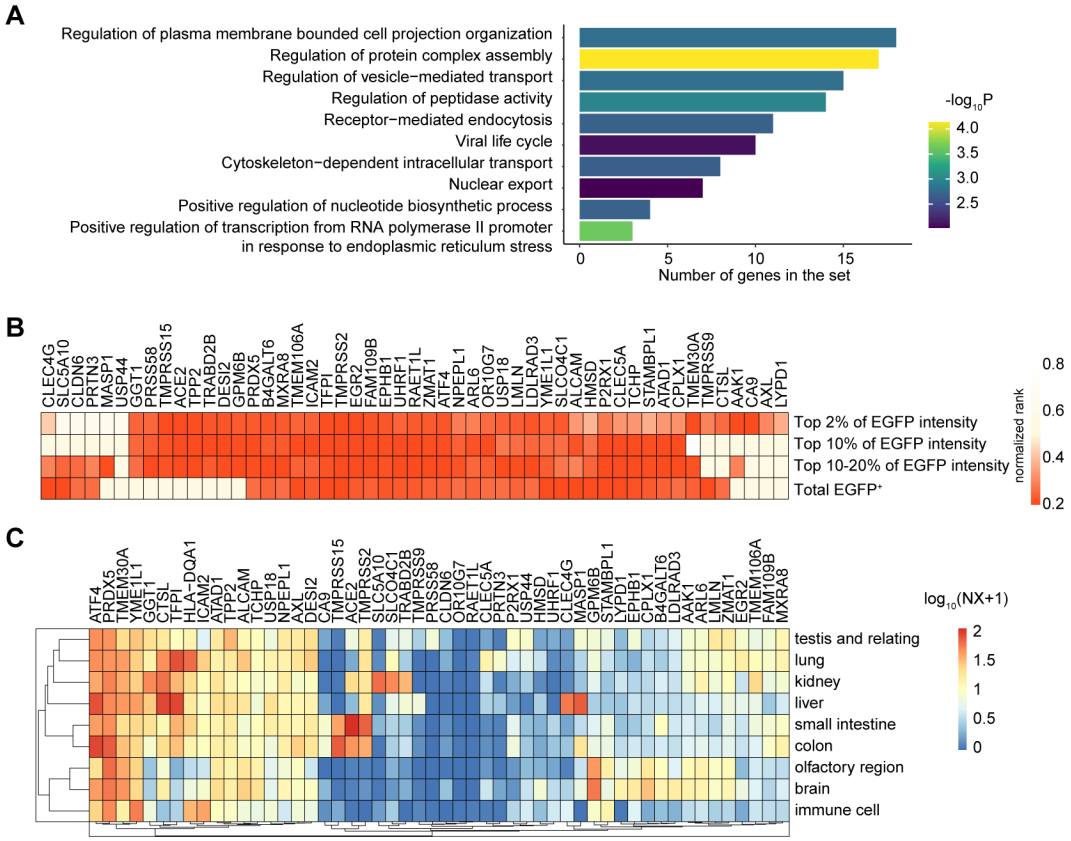

Fig. 2. Host factors identified from CRISPRa library screening. (**A**) Gene Ontology (GO) enrichment analysis was conducted using all the significant candidates (RRA score < 0.001) identified in the four groups. Hypergeometric test was used to calculate all the *p*-values. The top-enriched GO terms were selected for visualization. The x axis represents the number of genes identified in the specific GO terms. A complete list of genes in each GO term is in table S3. (**B**) The performance of all the significant hits in four screening groups (top 2%, top 10%, top 10-20% of EGFP intensity and total EGFP^{+}). The gene with a smaller value of normalized rank (in redder colour) represented a higher enrichment in the relevant groups. (**C**) Expression patterns of identified candidates within human tissues. The data used for analysis were retrieved from the Human Protein Atlas normalized expression.

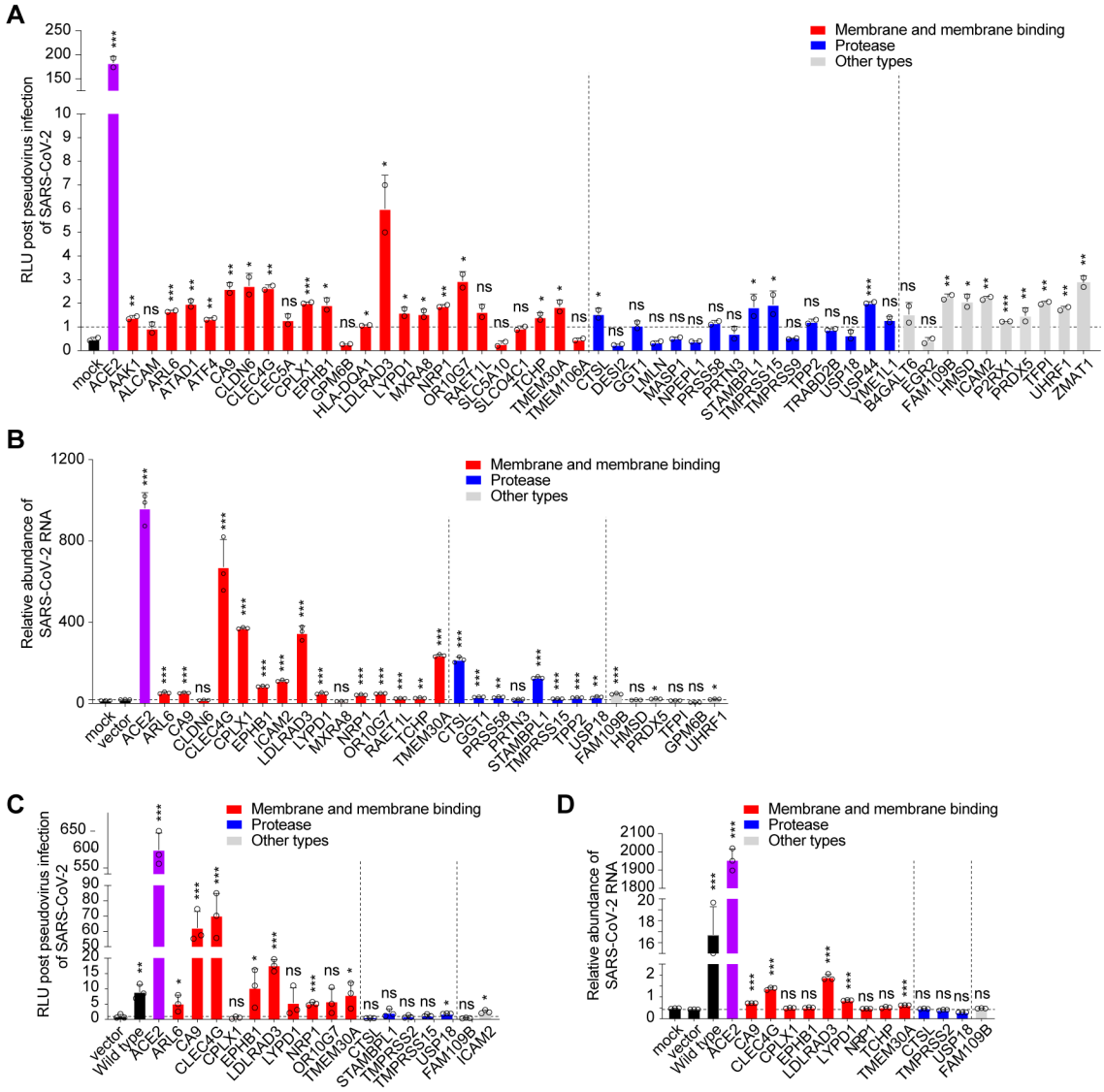

Fig. 3. Validation of candidate genes identified from CRISPRa library screening. (**A** and **B**) Effects of identified genes on the infection of SARS-CoV-2. (**A**) 51 individual cDNAs and an empty vector were transfected into HEK293T cells. Then the cells were treated with luciferase-labelled SARS-CoV-2 pseudotyped virus. The entry of SARS-CoV-2 pseudotyped virus was quantified through measuring luciferase activity 48 h later. The luciferase activities were normalized by the empty vector. Data are presented as the mean ± s.d. (n = 2). (**B**) The cDNAs of candidate genes were introduced into HEK293T cells lentivirally labelled with an mCherry marker. The mCherry-positive cells were enriched through FACS followed by infection with authentic SARS-CoV-2 virus at an MOI of 0.5. SARS-CoV-2 RNAs were quantified by real-time qPCR and normalized by *GAPDH*. Data were presented as the mean ± s.d. (n = 3). (**C** and **D**) Effects of identified genes on the infection of SARS-CoV-2 in *ACE2*$^{-/-}$ cells. (**C**) The

300 cDNAs were transfected into HEK293T *ACE2*$^{-/-}$ cells. Then the cells were treated with 10-fold
301 concentrated SARS-CoV-2 pseudotyped virus. The entry of pseudotyped virus was quantified through
302 measuring luciferase activity and was normalized by the empty vector. (**D**) The cDNAs of candidate
303 genes were introduced into HEK293T *ACE2*$^{-/-}$ cells lentivirally. Cells were enriched through FACS
304 followed by infection with authentic SARS-CoV-2 virus at an MOI of 0.5. SARS-CoV-2 RNAs were
305 quantified by real-time qPCR and normalized by *GAPDH*. Data were presented as the mean ± s.d. (n =
306 3). *P* values were calculated using Student's *t* test, **P* < 0.05; ***P* < 0.01; ****P* < 0.001; ns, not
307 significant.
308

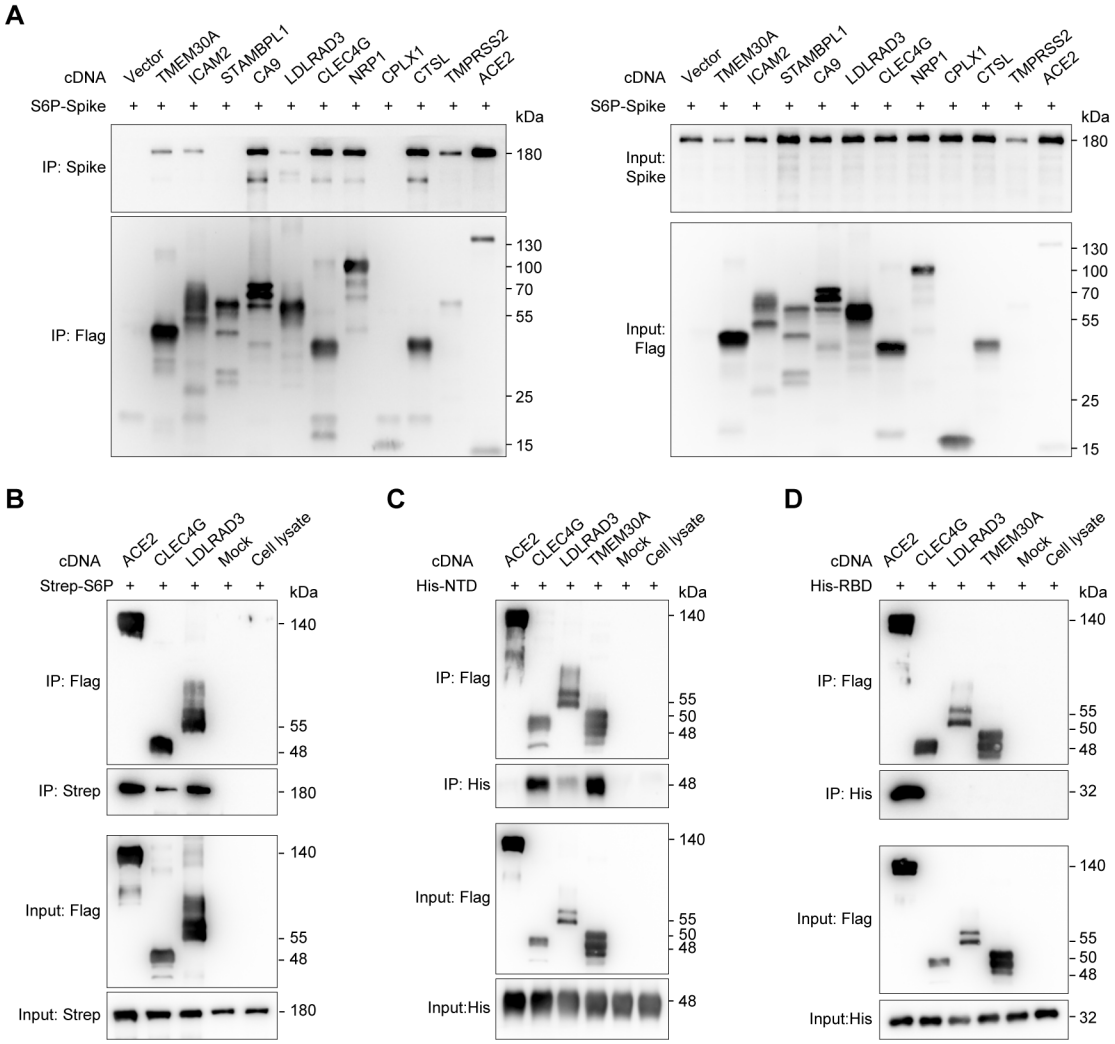

Fig. 4. Direct binding of LDLRAD3, CLEC4G and TMEM30A to SARS-CoV-2 S. (**A**) Co-IP of SARS-CoV-2 S6P spike with FLAG-tagged proteins in HEK293T cells transfected with Flag-cDNA constructs and SARS-CoV-2 S. Immunoblot analysis was conducted using anti-Flag and anti-spike antibodies. (**B**) *In vitro* pull-down assay of purified ACE2, CLEC4G and LDLRAD3 to SARS-CoV-2 S. Strep-tagged SARS-CoV-2 S and FLAG-tagged full-length candidate receptors were expressed in HEK293T cells and affinity-purified. Immunoblot analysis was conducted using anti-Flag and anti-Strep antibodies. (**C** and **D**) *In vitro* pull-down assay of purified ACE2, CLEC4G, LDLRAD3 and TMEM30A to the NTD (**C**) or RBD (**D**) of SARS-CoV-2 S. Immunoblot analysis was conducted using anti-Flag and anti-His antibodies.

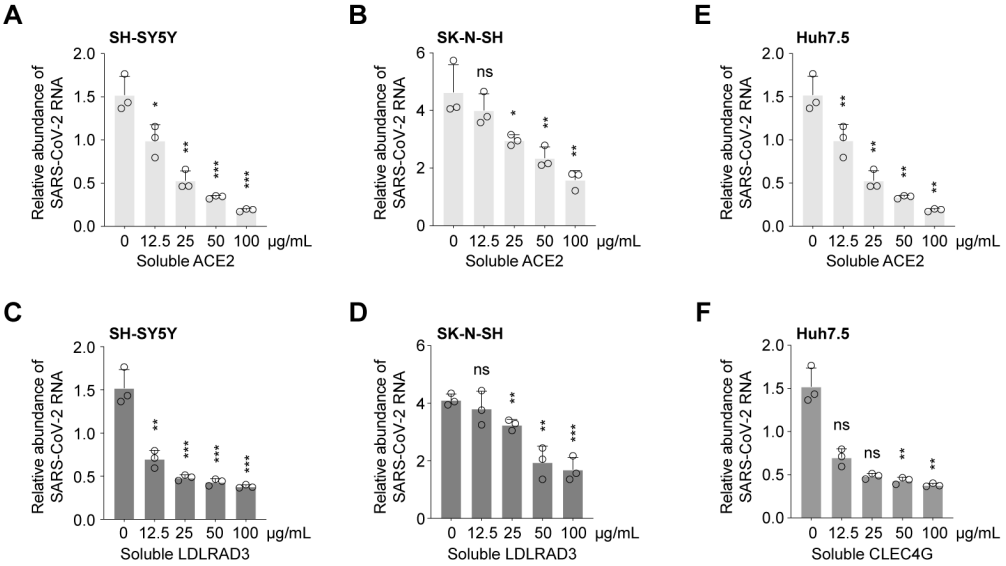

Fig. 5. Inhibition of soluble proteins on SARS-CoV-2 infection. (**A** and **B**) Effects of purified ACE2 on SARS-CoV-2 infection in SH-SY5Y (**A**) and SK-N-SH (**B**) cells. (**C** and **D**) Effects of purified LDLRAD3 on SARS-CoV-2 infection in SH-SY5Y (**C**) and SK-N-SH (**D**) cells. (**E** and **F**) Effects of purified ACE2 (**E**) and CLEC4G (**F**) on SARS-CoV-2 infection in Huh7.5 cells. The soluble proteins (0, 12.5, 25, 50 and 100 μg/mL) were incubated with authentic SARS-CoV-2 virus for 1 h. Infection was performed at an MOI of 0.5. SARS-CoV-2 RNAs were quantified by real-time qPCR and normalized by *GAPDH*. Data were presented as the mean ± s.d. (n = 3). *P* values were calculated using Student's *t* test, **P* < 0.05; ***P* < 0.01; ****P* < 0.001; ns, not significant.

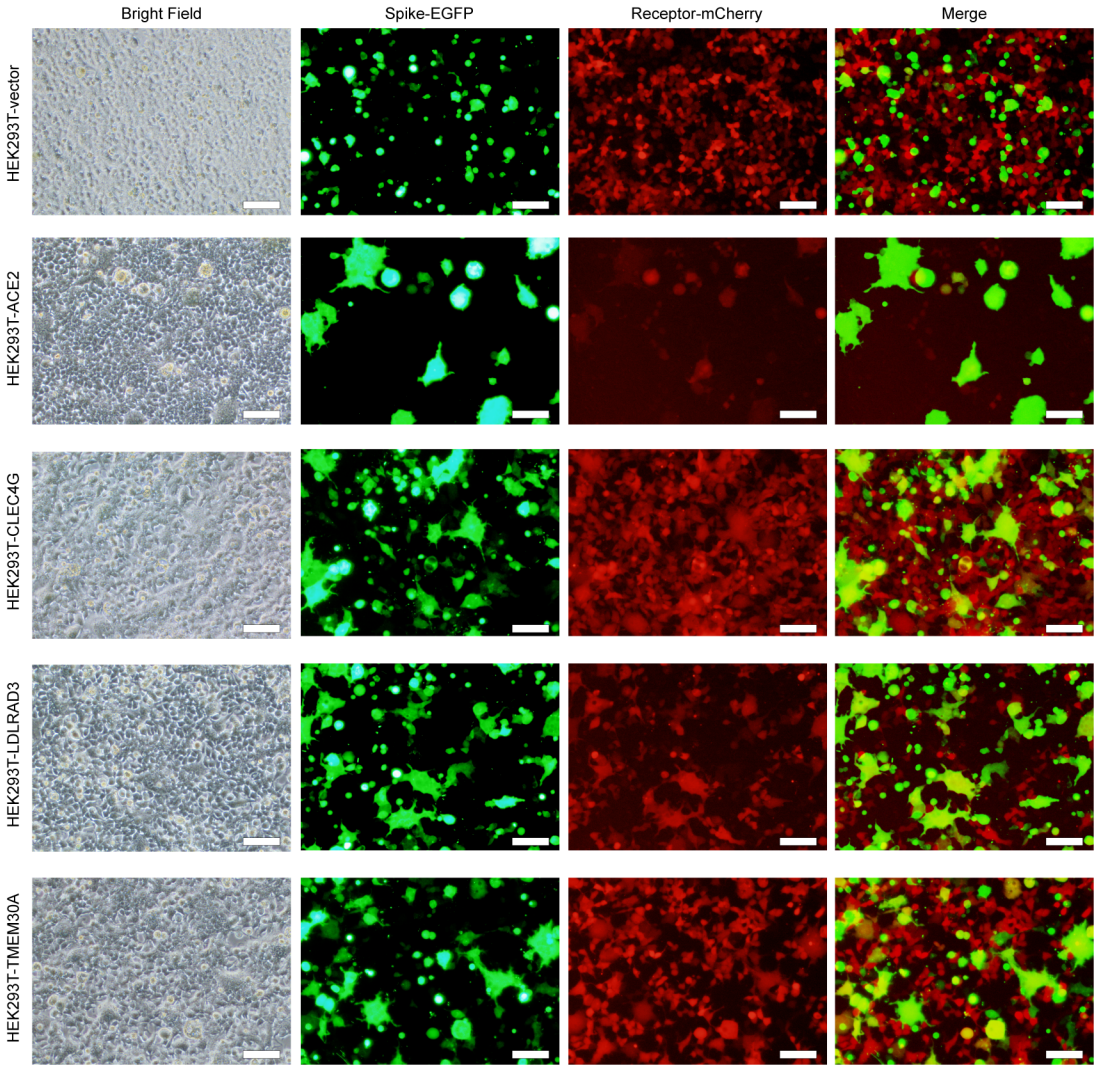

Fig. 6. Examination of the interaction between SARS-CoV-2 S protein and candidate receptors by syncytium formation assay. Spike-EGFP represents the HEK293T cells transfected with SARS-CoV-2 S protein and an EGFP marker. Receptor-mCherry represents the HEK293T cells stably overexpressed with the known and candidate receptors labelled with an mCherry marker, labeled as HEK293T-ACE2, HEK293T-CLEC4G, HEK293T-LDLRAD3 and HEK293T-TMEM30A. HEK293T cells infected with the cDNA-expressing vector, labeled as HEK293T-vector, was served as the control. Merge indicates the co-localization of the two categories of cells through merging the EGFP and mCherry fluorescence channels by ImageJ. The images were taken 40 h after co-culturing the two categories of cells. The scale bar = 100 μm.

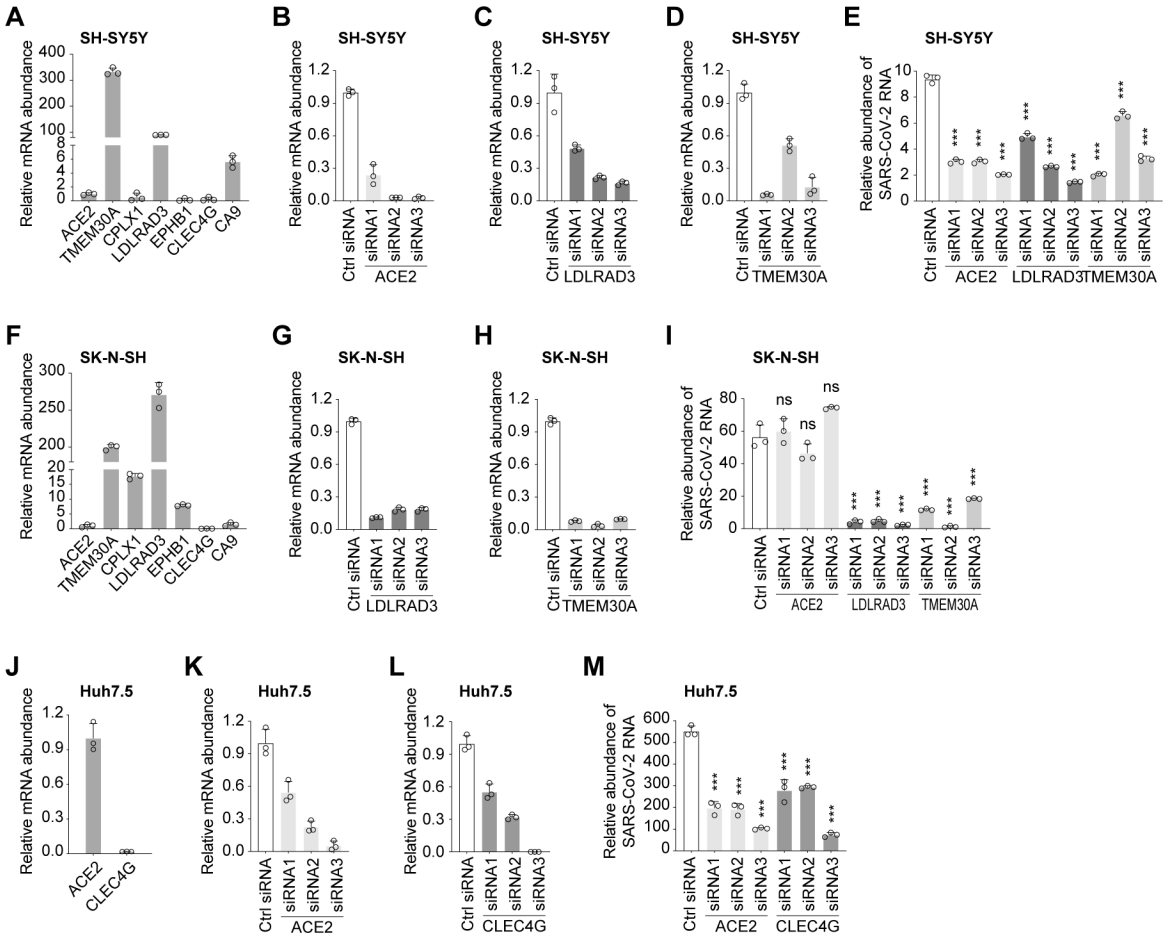

Fig. 7. Loss-of-function effects of identified receptors on SARS-CoV-2 infection. (**A**) Expression of identified host factors relative to *ACE2* in SH-SY5Y cells. (**B** to **D**) Suppression of *ACE2* (**B**), *LDLRAD3* (**C**) and *TMEM30A* (**D**) by siRNAs in SH-SY5Y cells. (**E**) Effects of suppression of candidate receptors by siRNAs on SARS-CoV-2 infection in SH-SY5Y cells. Infection was performed at an MOI of 0.5. (**F**) Expression of identified host genes relative to *ACE2* in SK-N-SH cells. (**G** and **H**) Suppression of *LDLRAD3* (**G**) and *TMEM30A* (**H**) by siRNAs in in SK-N-SH cells. (**I**) Effects of suppression of candidate genes by siRNAs on SARS-CoV-2 infection in SK-N-SH cells. Infection was performed at an MOI of 0.5. (**J**) Expression of identified host genes relative to *ACE2* in Huh7.5 cells. (**K** and **L**) Suppression of *ACE2* (**K**) and *CLEC4G* (**L**) by siRNAs in in Huh7.5 cells. (**I**) Effects of suppression of candidate genes by siRNAs on SARS-CoV-2 infection in Huh7.5 cells. Infection was performed at an MOI of 0.5. For all these experiments, a total of 20 pmol for each siRNA was transfected into cells. The relative mRNA abundance was quantified 48 h post transfection. Ctrl RNA: Random non-targeting siRNA. RNA abundance of host factors and SARS-CoV-2 were quantified by real-time qPCR and normalized by *GAPDH*. Data were presented as the mean ± s.d. (n = 3). *P* values

356 were calculated using Student's *t* test, *$P < 0.05$; **$P < 0.01$; ***$P < 0.001$; ns, not significant. Primers
357 used for real-time qPCR were listed in table S5.
358

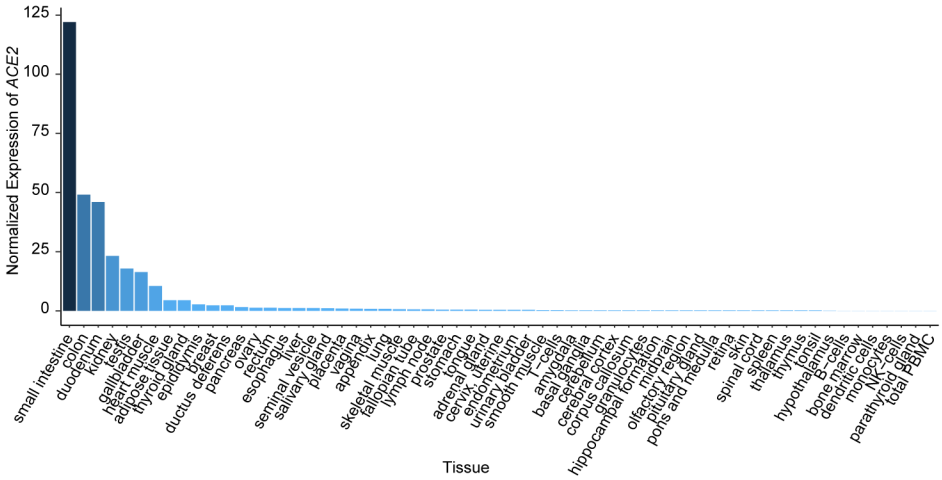

fig. S1. Normalized *ACE2* expression levels in different human tissues. The data used for analysis were retrieved from Human Protein Atlas normalized expression.

363

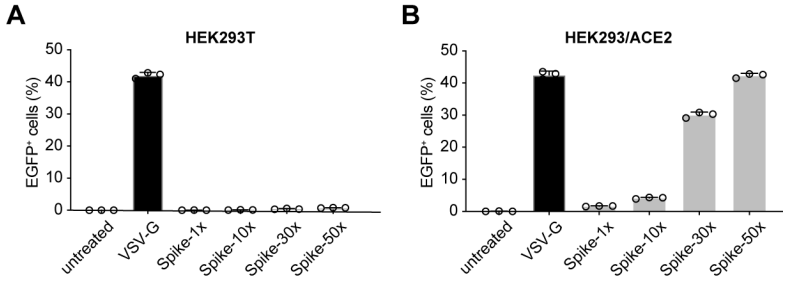

364 **fig. S2. Examination of the approach in simulating SARS-CoV-2 infection using the SARS-CoV-2**
365 **pseudotyped virus.** (**A**) Examination of the virus infection in wild type HEK293T cells using different
366 concentrations of pseudovirus. HEK293T cells were respectively infected with 1-fold (Spike-1×), 10-
367 fold (Spike-10×), 30-fold (Spike-30×) and 50-fold (Spike-50×) concentrated pseudovirus harboring
368 SARS-CoV-2 S protein, and the $EGFP^+$ percentages were analyzed by FACS 48 h post infection. The
369 lentivirus harboring VSV-G protein was used for infection as a positive control following the same
370 procedure. (**B**) Examination of the concentration of pseudovirus for achieving an efficient virus infection
371 in HEK293 cells stably expressing *ACE2*.
372

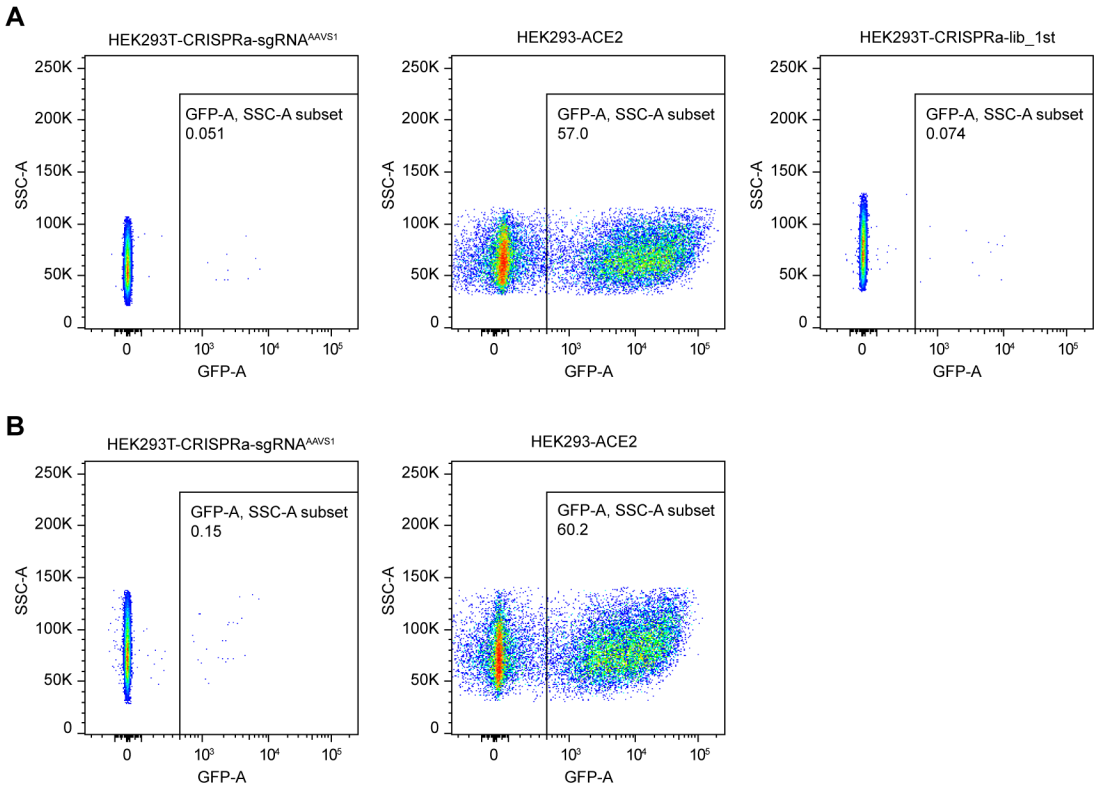

fig. S3. FACS selection of EGFP$^+$ cells in each round of screening after SARS-CoV-2 pseudovirus infection. (**A**) The first FACS selection of EGFP$^+$ cells from the HEK293T-CRISPRa library cells. Left: HEK293T-CRISPRa cells stably expressing *AAVS1*-targeting sgRNA were infected with SARS-CoV-2 pseudovirus (50-fold), serving as the negative control; Middle: HEK293 cells stably expressing ACE2 were infected with SARS-CoV-2 pseudovirus, serving as the positive control; Right: HEK293T-CRISPRa library cells were infected with SARS-CoV-2 pseudovirus for the first round. (**B**) The controls used in the second round of FACS selection of EGFP$^+$ cells. The negative and positive controls were the same as in fig. S2A (left and middle), and the FACS selection of library cells for the second round was presented in Fig.1D.

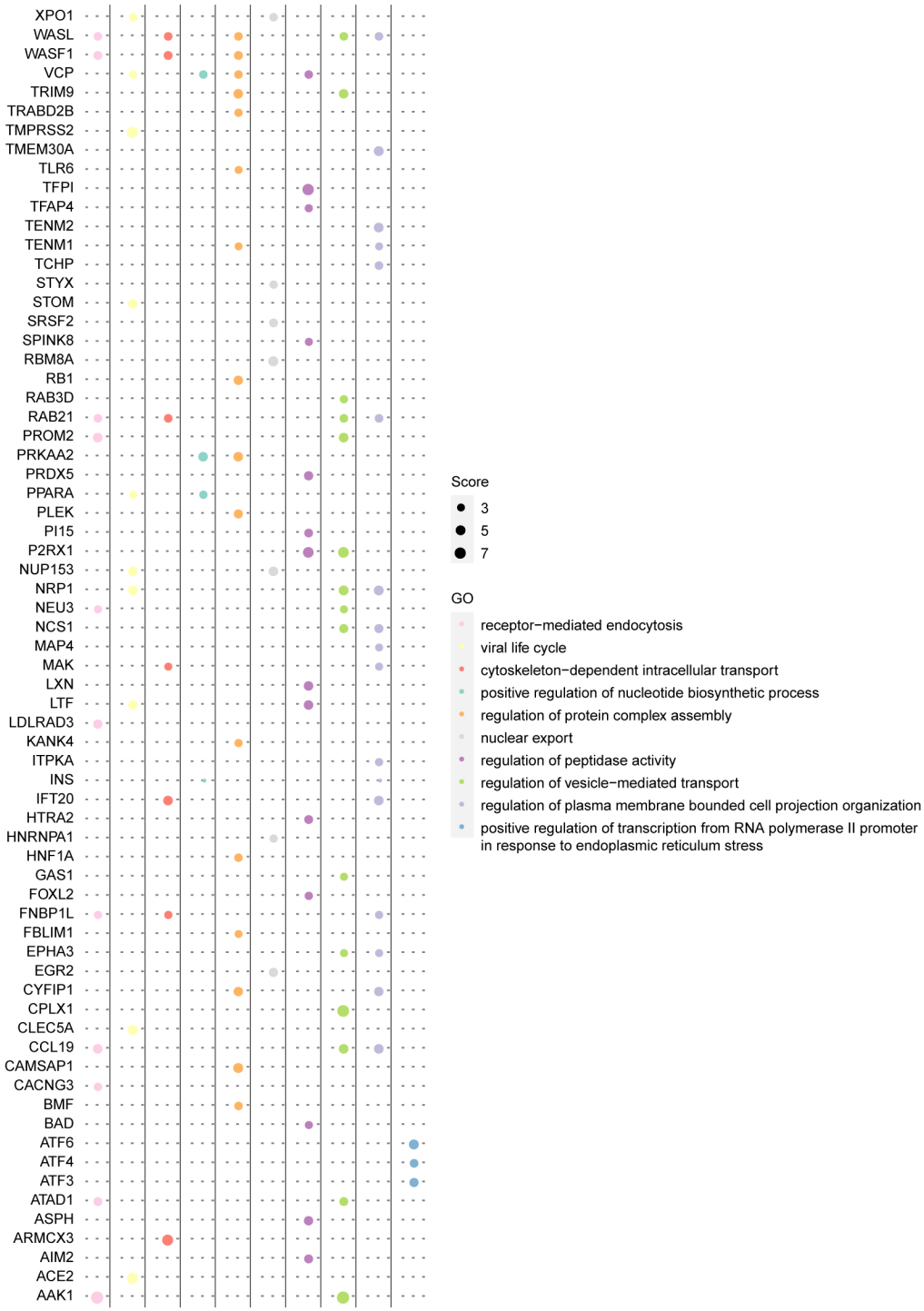

fig. S4. The total gene list from GO enrichment analysis. The size of round dots indicated scores of CRISPRa screening.

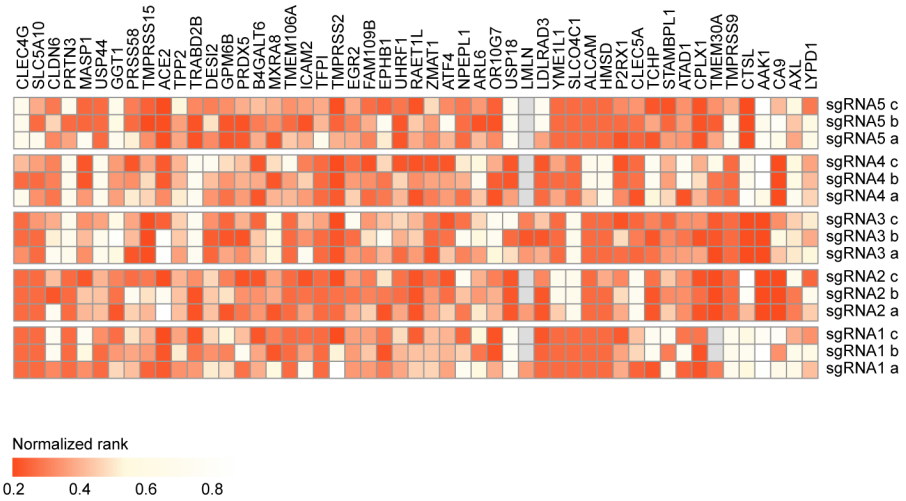

fig. S5. The performance of all the sgRNAs^{eBAR} targeting the identified candidates. Three eBARs of each sgRNA were indicated by a, b and c.

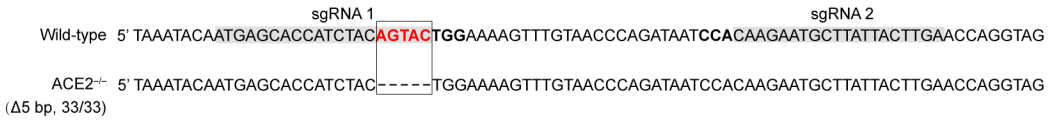

fig. S6. Partial coding sequences of the *ACE2* gene in the genome containing the sgRNA binding regions. The sequencing analysis of the mutated alleles were obtained from 33 randomly selected clones. The dashes indicate deletions.

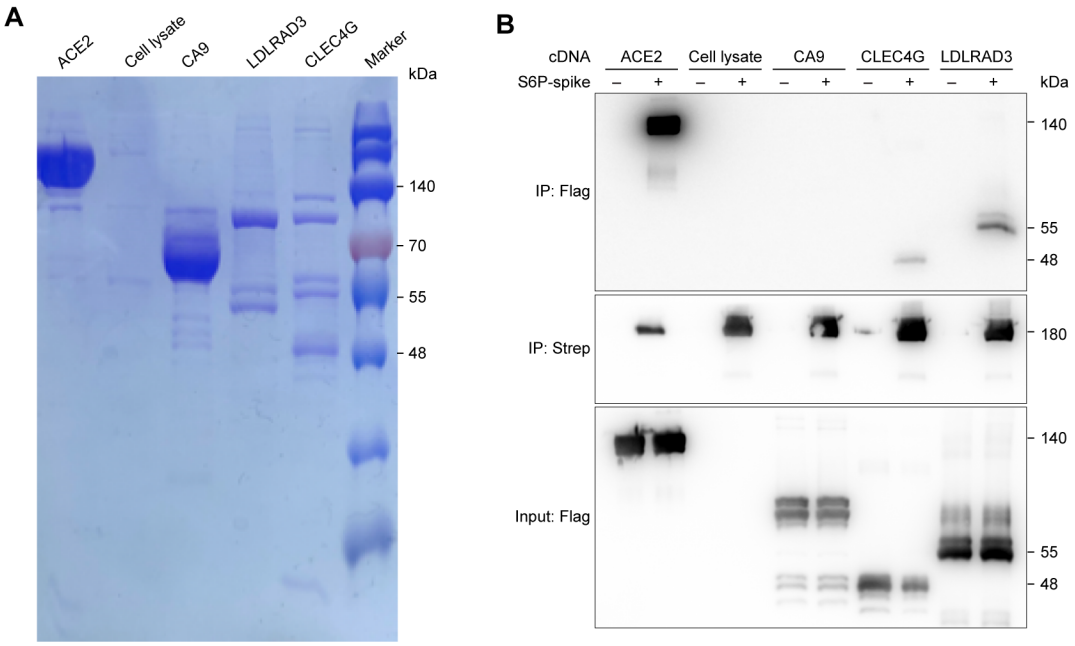

397

398 **fig. S7. Direct binding of identified proteins to SARS-CoV-2 S.** (**A**) Flag-tagged CA9, LDLRAD3,
399 CLEC4G and ACE2 were purified and shown on a Coomassie blue-stained SDS-PAGE gel. (**B**) *In vitro*
400 pull-down assay of purified ACE2, CA9, CLEC4G and LDLRAD3 to SARS-CoV-2 S. Strep-tagged
401 SARS-CoV-2 S and FLAG-tagged candidate receptors were expressed in HEK293T cells and affinity-
402 purified. Immunoblot analysis was conducted using anti-Flag and anti-Strep antibodies.
403

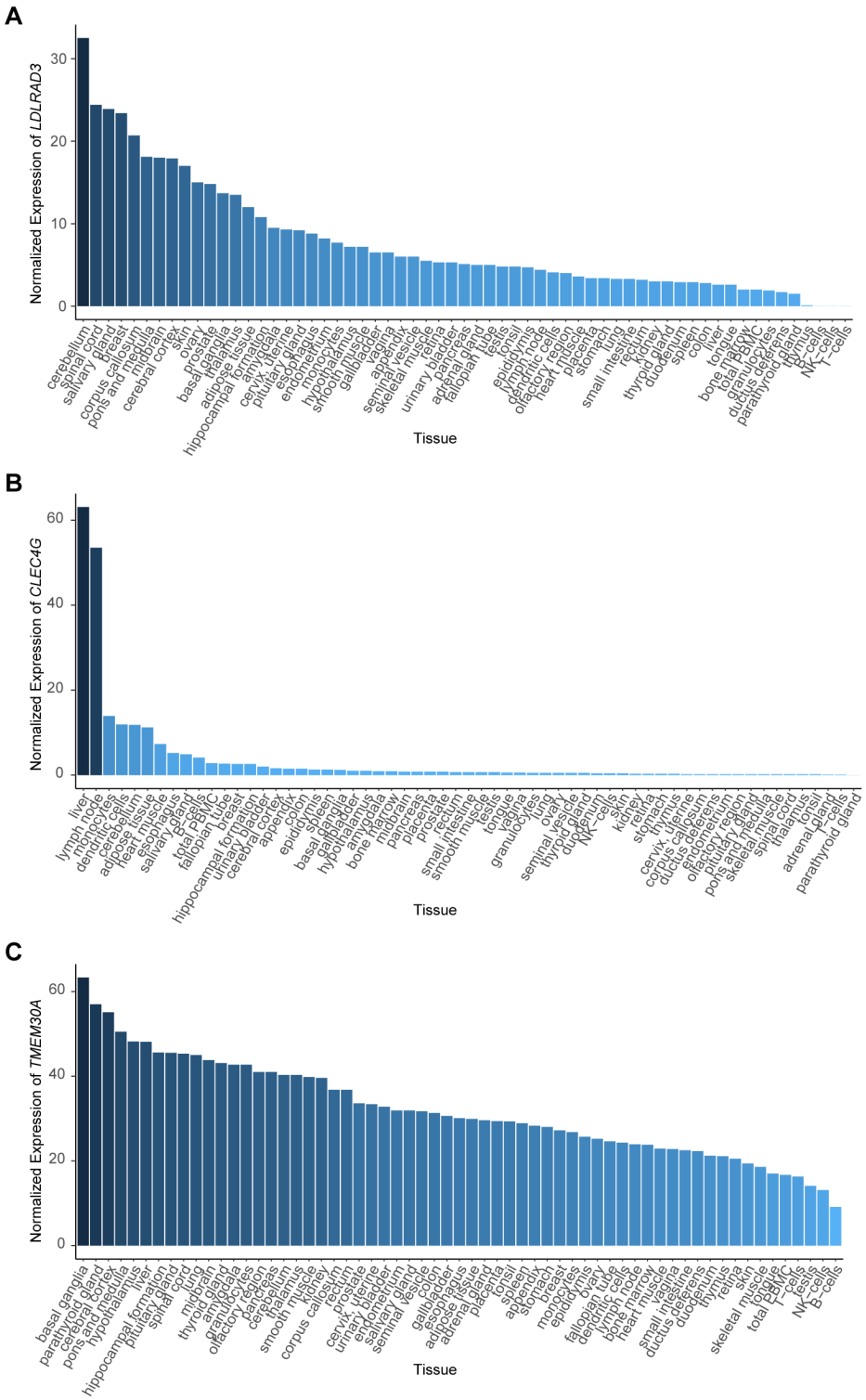

fig. S8. **Expression patterns of candidate receptors within human tissues.** The mRNA levels of *LDLRAD3* (**A**), *CLEC4G* (**B**) and *TMEM30A* (**C**) within human tissues were analysed using data retrieved from Human Protein Atlas.

408 **Materials and Methods**

409

410 **Plasmids**

411 The lentiviral sgRNA^{eBAR}-expressing backbone was constructed by inserting sgRNA scaffold embedded
412 MS2 loops at tetraloop and stemloop 2 along with eBAR sequence into pLenti-sgRNA-Lib (Addgene,
413 53121). The sgRNA-expressing sequences were cloned into the backbone using the BsmBI-mediated
414 Golden Gate cloning strategy (*47*). The pLenti-EGFP used for pseudovirus production was constructed
415 by cloning EGFP sequence into pLenti-SV40-mCherry. The cDNA-expressing plasmids were
416 constructed by inserting each cDNA sequence into the multiple cloning sites before the Flag tag of the
417 pLenti-SV40-mCherry vector following the standard cloning protocol. The plasmids lenti dCAS-
418 VP64_Blast (Addgene, 61425) and lenti MS2-P65-HSF1_Hygro (Addgene, 61426) were purchased
419 from Addgene. The oligos of CRISPRa library were synthesized in Synbio Technologies according to
420 the Human Genome-wide CRISPRa-v2 Libraries (Addgene, 83978) (*30*).

421

422 **Cell culture**

423 The HEK293T cell line was from EdiGene Inc., and Huh 7.5 cell line was from S. Cohen's laboratory
424 (Stanford University School of Medicine). All these cells were maintained in Dulbecco's modified
425 Eagle's medium (DMEM; Gibco, C11995500BT) supplemented with 10% fetal bovine serum (FBS;
426 Biological Industries, 04-001-1ACS) and 1% penicillin/streptomycin, and cultured with 5% CO2 at
427 37°C. Sf21 insect cells were maintained in SIM SF medium (Sino Biological, RZ13NO0801) and 1%
428 penicillin/streptomycin (Gibco, 2257215) with 110 rpm at 27°C. All cells were routinely checked to
429 confirm the absence of mycoplasma contamination.

430

431 **Production and infection of SARS-CoV-2 pseudotyped virus**

432 HEK293T cells were seeded 24 h before pseudovirus packaging. The SARS-CoV-2 pseudotyped virus
433 was generated by co-transfection of the pCAGGS-S with the viral packaging plasmid psPAX2 and
434 pLenti-EGFP/luciferase-expressing plasmid as a proportion of 1:1:1 into HEK293T cells using the X-
435 tremeGENE HP DNA transfection reagent (Roche, 06366546001) according to the manufacturer′s
436 instructions. The cell supernatant containing pseudovirus was collected 48 h post transfection, and was
437 directly concentrated in different ratios using Lenti-X™ Concentrator (Clontech, 631232). The
438 concentrated pseudovirus was immediately added into cells for infection without freez-thawing. For

439 infection with SARS-CoV-2 pseudotyped virus, cells were seeded 24 h before virus collecting.
440 Concentrated pseudovirus was added into culturing medium with polybrene (8 μg/mL). After 24 h, the
441 medium was changed by conventional medium and cells were incubated for another 48 h.
442
443 **Construction of the CRISPRa sgRNA^{eBAR} plasmid library**
444 The synthesized oligo pool of CRISPRa library was PCR amplified with primers (table S5) including the
445 BsmBI recognition sites using Phusion®High-Fidelity PCR Kit (NEB, E0553L). After purification with
446 DNA Clean & Concentrator-25 (Zymo Research Corporation, D4034), the purified PCR product was
447 respectively inserted into the three sgRNA^{eBAR}-expressing backbones constructed above through the
448 Golden Gate cloning strategy (*47*). The ligation mixture of each group was separately purified with
449 DNA Clean & Concentrator-5 (Zymo Research Corporation, D4014), and was electro-transformed into
450 E.coli HST08 Premium Electro-Cells (Takara, 9028) according to the manufacturer's protocol using a
451 Gene Pulser Xcell (BioRad). Transformed clones were counted to ensure at least 300-fold coverage for
452 each sgRNA^{eBAR}. The plasmid of each sgRNA^{eBAR} library was extracted using an EndoFree Plasmid
453 Maxi Kit (QIAGEN, 12362), and further mixed in a 1:1:1 molar ratio. The library lentivirus was
454 generated by co-transfection of the library plasmid mixture with two lentiviral packaging plasmids
455 pR8.74 and pVSV-G (Addgene, 12259) as a proportion of 10:10:1 into HEK293T cells. The cell
456 supernatant containing lentivirus was collected 48 h post transfection and stored at -80°C.
457
458 **CRISPRa screening for SARS-CoV-2 entry factors**
459 The HEK293T cells were engineered to stably express the CRISPRa system including lenti dCAS-
460 VP64_Blast and lenti MS2-P65-HSF1_Hygro vectors, termed as HEK293T-CRISPRa cells. The
461 HEK293T-CRISPRa cells were seeded 24 h post lentiviral infection, and were further infected with the
462 library lentivirus at an MOI of 10 with a high coverage (5000-fold) for each sgRNA. Two days post
463 lentiviral infection, the library cells were subjected to puromycin selection for 48 h (1 μg/mL). After
464 puromycin treatment, the library cells were collected as the reference sample and were continuously
465 cultured for 5 days. The fresh SARS-CoV-2 pseudovirus with EGFP marker (50-fold) was added to the
466 library cells, and the EGFP positive cells were sorted by FACS 48 h post first round of pseudovirus
467 infection. After culturing the sorted cells for additional several days, a second round of pseudovirus
468 infection were conducted as described above, and the library cells were sorted for total EGFP^{+} cells as
469 well as the top 10-20%, top 10% and top 2% grouped by the EGFP intensity. The reference sample and

470 each group of $EGFP^+$ cells were subjected to genomic extraction (QIAGEN, 69506), PCR amplification
471 of the $sgRNA^{eBAR}$ sequences (KAPA, KK2625) and high-throughput sequencing as previously described
472 (*48*).
473
474 **Analysis of CRISPRa screening results**
475 In order to calculate the enriched genes after CRISPRa screening, we developed an analysis algorithm
476 eBAR-analyzer, which was implemented using R and could be obtained from
477 https://github.com/wolfsonliu/FluorescenceSelection. In principle, the eBAR-analyzer algorithm adopt
478 binomial distribution, in which the selection of cells hosting sgRNAs targeting specific genes enriched
479 by FACS was considered as results of series of Bernoulli trials. The normalization of raw counts of
480 $sgRNAs^{eBAR}$ was calculated based on the cell proportion of EGFP intensity groups compared with the
481 initial cell population. For instance, when we selected the top 2% intensity of $EGFP^+$ cells, the
482 normalization factor for the group will be 0.02. Then the normalized counts would be total detected
483 reads multiplied by group normalization factor. The final normalization process would ensure that the
484 smallest normalized counts will be an integer after rounded. Based on this, the *p*-values of the
485 $sgRNAs^{eBAR}$ were calculated by assuming counts of each intensity group were drawn from the initial
486 population counts satisfying a binomial distribution. The normalized ranks of *p*-values for each
487 $sgRNA^{eBAR}$ were calculated. Finally, Robust Rank Aggregation (RRA) (*49*) was used to calculate the
488 rank in gene level from the normalized ranks of *p*-values of $sgRNAs^{eBAR}$. The RRA scores were the
489 output results of the algorithm.
490
491 **GO enrichment and expression pattern analysis**
492 The Gene Ontology (GO) enrichment analysis of identified host factors (RRA score < 0.001) was
493 performed using Metascape Resource (*32*). Hypergeometric test was used to calculate all the *p*-values
494 for all the terms. We selected top-enriched GO terms for visualization in this manuscript. For the
495 expression pattern analysis of identified candidates, we use data retrieved from Human Protein Atlas to
496 obtain normalized expression of each factor (*42*).
497
498 **Validation of identified candidates**
499 For the individual validation of screening results, we introduced cDNAs of candidate genes into cells.
500 The cDNAs were transfected into cells using the X-tremeGENE HP DNA transfection reagent (Roche,

501 06366546001). Then the transfected cells were infected by concentrated SARS-CoV-2 pseudotyped
502 virus 48 h later. The infection of pseudotyped virus was quantified through measuring luciferase
503 activities.
504
505 The lentiviral particles expressing individual cDNA labelled with an mCherry marker were generated by
506 co-transfection of the cDNA plasmid mixture with two lentiviral packaging plasmids pR8.74 and pVSV-
507 G (Addgene, 12259) as a proportion of 10:10:1 into HEK293T cells, followed by infection into cells.
508 The cDNA transduced cells were selected through FACS and were infected with authentic SARS-CoV-2
509 virus at an MOI of 0.5 for 1 h. Infected cells were cultured for another 24 h with conventional medium,
510 then treated with Trizol. The infection of authentic SARS-CoV-2 virus was quantified by real-time
511 qPCR of RNA abundance.
512
513 **Protein production and purification**
514 The SARS-CoV-2 NTD (residues 13-303) or RBD (residues 319-541) with a C-terminal His tag was
515 cloned into a modified pFastBac vector (Invitrogen) that encodes a melittin signal peptide before the
516 NTD or RBD. Bacmids DNA were generated using the Bac-to-Bac system. Baculoviruses were
517 generated and amplified using the Sf21 insect cells, and were subsequently used to infect High Five
518 insect cells for protein expression. NTD/RBD was retrieved from the conditioned cell growth media
519 using the Ni-NTA resin and further purified using a Superdex 200 Increase 10/300 gel filtration column
520 in 20 mM HEPES pH 7.2, and 150 mM NaCl. Strep-tagged S6P spike protein was expressed in the
521 HEK293F cells and purified as described previously (*50*).
522
523 **Co-IP**
524 For the Co-IP assay, the plasmids of SARS-CoV-2 S6P spike and individual cDNA were transfected
525 into HEK293T cells. After 48 h, the cells were washed using precooled PBS for 3 times, then lysed with
526 precooled lysis buffer (50 mM Tris-HCl pH 7.4, 150 mM NaCl, 0.25% Na-deoxycholate, 1 mM EDTA,
527 1% NonidetP-40) with Protease Inhibitor Cocktail Tablet (Thermo, VJ313124) at 4 °C for 1 h before
528 being subjected to centrifugation at 15, 000 g at 4°C for 15 min. We transferred 30 μL sample into a
529 new tube as the input. The rest of cell lysates were treated with Anti-Flag M2 Affinity Gel (Sigma,
530 A2220) at 4°C overnight. Then the lysates were washed using wash buffer (50 mM Tris-HCl pH 7.4,
531 150 mM NaCl, 0.25% Na-deoxycholate, 1 mM EDTA, 0.1% NonidetP-40) for at least 4 times. The

532 proteins were eluted using 250 μg/mL Flag peptide into wash buffer for 1 h at 4°C and subjected to
533 immunoblotting analysis using antibodies for Flag tag (SIGMA, SLCD6338) and SARS-CoV-2 S (Sino
534 Biological, 40589-T62).
535
536 **Flag pull-down assay**
537 Potential receptor proteins with C-terminal Flag tag were transiently expressed in HEK293F cells using
538 polyethylenimine (PEI, Polysciences). 36 h following transfection, the cells were collected by
539 centrifugation and disrupted on ice using a dounce homogenizer in the lysis buffer [25 mM Tris pH 8.0,
540 150 mM NaCl, 1.0% (w/v) N-dodecyl β-d-maltoside (DDM), and 0.1% (w/v) cholesterol hemisuccinate
541 (CHS)], supplemented with Protease Inhibitor cocktail (Bimake, B14001). After ultracentrifugation (45,
542 000 g, 30 min, 4°C), the supernatants were first incubated with the anti-Flag affinity beads (Smart-
543 Lifesciences, SA042025) for 2 h at 4°C with rotation. The beads were then pelleted and washed for five
544 times with the wash buffer [25 mM Tris pH 8.0, 150 mM NaCl, 0.3% (w/v) DDM, and 0.03% (w/v)
545 CHS]. Afterwards, the beads were incubated with purified S6P/NTD/RBD proteins as described above
546 for 1 h with rotation. The beads were then again pelleted and washed five times with the wash buffer.
547 Bound proteins were eluted from the beads using the elute buffer [25 mM Tris pH 8.0, 150 mM NaCl,
548 0.1% (w/v) DDM, 0.01% (w/v) CHS, and 250 ng/mL Flag peptide], and analyzed by immunoblotting
549 using antibodies for the Strep tag (HuaxingBio, HX1816) or His tag (TransGen, HT501).
550
551 **StrepTactin pull-down assay**
552 For the StrepTactin pull-down assay, potential receptor proteins were purified using the anti-Flag
553 affinity beads and eluted as described above. Then they were incubated with purified S6P on ice for 1 h.
554 The mixtures were then incubated with the StrepTactin beads (Smart Lifesciences) in the wash buffer at
555 4°C for another 1 h with rotation, washed by five times with the wash buffer, and eluted using the final
556 buffer [25 mM Tris pH 8.0, 150 mM NaCl, 0.1% (w/v) DDM, 0.01% (w/v) CHS, and 10 mM
557 desthiobiotin]. The results were analyzed by immunoblotting using antibodies for the Flag tag (SIGMA,
558 SLCD6338).
559
560 **Syncytium formation assay**
561 HEK293T cells were first transfected with the pCAGGS-S plasmid with an EGFP selection marker. 24 h
562 post transfection, the transfected cells were detached, and mixed with HEK293T cells stably

563 overexpressing different cDNAs (ACE2, CLEC4G, LDLRAD3, TMEM30A and the cDNA-expressing
564 empty vector as the negative control) labelled with an mCherry marker in a 1:1 ratio. Then the two
565 categories of cells were co-cultured in 12-well plates at about 60% confluency. After 40 h of cell co-
566 culture, the images were captured by fluorescence microscopy.
567
568 **Real-time qPCR**
569 The cultured cells transfected with siRNAs or/and infected with authentic SARS-CoV-2 virus were
570 treated by Trizol. RNA was extracted using Direct-zol RNA kit (Zymo, R2069), and the cDNA was
571 synthesized using QuantScript RT kit (TIANGEN, KR103-03). Real-time PCR was performed using
572 SYBR Premix Ex Taq II (TaKaRa, RR820A) on LightCycler96 qPCR system (Roche). The relative
573 RNA abundance of candidate factors or SARS-CoV-2 virus was measured and normalized by GAPDH.
574 All the primers used for real-time qPCR were listed in table S5.
575
576 **Inhibition of SARS-CoV-2 infection by soluble proteins and siRNAs**
577 For inhibition by soluble proteins, the purified protein of ACE2, LDLRAD3 or CLEC4G with different
578 doses (0, 12.5 μg/mL, 25 μg/mL, 50 μg/mL and 100 μg/mL) were incubated with authentic SARS-CoV-
579 2 virus for 1 h followed by infection at an MOI of 0.5. For inhibition by siRNAs, cells were seeded at
580 24-well plates 24 h before transfection. Each siRNA including negative control siRNA at an amount of
581 20 pmol was transfected into cells with 6 μL Lipofectamine RNAiMAX Reagent (Life technologies,
582 13778-150). 24 h later, the cells were infected with authentic SARS-CoV-2 virus at an MOI of 0.5 for 1
583 h. Infected cells were cultured for another 24 h with conventional medium, then treated with Trizol. The
584 infection of authentic SARS-CoV-2 virus was quantified by real-time qPCR of RNA abundance.
585
586 **Statistical analysis**
587 Statistical analysis of all data apart from CRISPRa screening was performed using GraphPad Prism
588 software. The statistical significance was evaluated using Student's *t* test and determined as $p < 0.05$. *P*-
589 values were indicated in each of figure legends.
590
591

References and Notes

1. L. L. Ren *et al.*, Identification of a novel coronavirus causing severe pneumonia in human: a descriptive study. *Chin Med J (Engl)* **133**, 1015-1024 (2020).
2. N. Zhu *et al.*, A Novel Coronavirus from Patients with Pneumonia in China, 2019. *The New England journal of medicine* **382**, 727-733 (2020).
3. K. G. Andersen, A. Rambaut, W. I. Lipkin, E. C. Holmes, R. F. Garry, The proximal origin of SARS-CoV-2. *Nat Med* **26**, 450-452 (2020).
4. D. Wang *et al.*, Clinical Characteristics of 138 Hospitalized Patients With 2019 Novel Coronavirus-Infected Pneumonia in Wuhan, China. *Jama* **323**, 1061-1069 (2020).
5. C. Huang *et al.*, Clinical features of patients infected with 2019 novel coronavirus in Wuhan, China. *Lancet* **395**, 497-506 (2020).
6. J. Helms *et al.*, Neurologic Features in Severe SARS-CoV-2 Infection. *The New England journal of medicine* **382**, 2268-2270 (2020).
7. V. G. Puelles *et al.*, Multiorgan and Renal Tropism of SARS-CoV-2. *The New England journal of medicine* **383**, 590-592 (2020).
8. K. S. Cheung *et al.*, Gastrointestinal Manifestations of SARS-CoV-2 Infection and Virus Load in Fecal Samples From a Hong Kong Cohort: Systematic Review and Meta-analysis. *Gastroenterology* **159**, 81-95 (2020).
9. M. Madjid, P. Safavi-Naeini, S. D. Solomon, O. Vardeny, Potential Effects of Coronaviruses on the Cardiovascular System: A Review. *JAMA Cardiol* **5**, 831-840 (2020).
10. P. Zhou *et al.*, A pneumonia outbreak associated with a new coronavirus of probable bat origin. *Nature* **579**, 270-273 (2020).
11. M. Hoffmann *et al.*, SARS-CoV-2 Cell Entry Depends on ACE2 and TMPRSS2 and Is Blocked by a Clinically Proven Protease Inhibitor. *Cell* **181**, 271-280 e278 (2020).
12. X. Ou *et al.*, Characterization of spike glycoprotein of SARS-CoV-2 on virus entry and its immune cross-reactivity with SARS-CoV. *Nature communications* **11**, 1620 (2020).
13. A. C. Walls *et al.*, Structure, Function, and Antigenicity of the SARS-CoV-2 Spike Glycoprotein. *Cell* **181**, 281-292 e286 (2020).
14. J. Shang *et al.*, Structural basis of receptor recognition by SARS-CoV-2. *Nature* **581**, 221-224 (2020).
15. S. Lukassen *et al.*, SARS-CoV-2 receptor ACE2 and TMPRSS2 are primarily expressed in bronchial transient secretory cells. *Embo J* **39**, e105114 (2020).
16. J. A. Aguiar *et al.*, Gene expression and in situ protein profiling of candidate SARS-CoV-2 receptors in human airway epithelial cells and lung tissue. *Eur Respir J* **56**, (2020).
17. R. A. Grant *et al.*, Circuits between infected macrophages and T cells in SARS-CoV-2 pneumonia. *Nature* **590**, 635-641 (2021).
18. X. Ren *et al.*, COVID-19 immune features revealed by a large-scale single-cell transcriptome atlas. *Cell* **184**, 1895-1913 e1819 (2021).
19. M. Puray-Chavez *et al.*, Systematic analysis of SARS-CoV-2 infection of an ACE2-negative human airway cell. *bioRxiv*, (2021).
20. S. Wang *et al.*, AXL is a candidate receptor for SARS-CoV-2 that promotes infection of pulmonary and bronchial epithelial cells. *Cell Res* **31**, 126-140 (2021).
21. J. L. Daly *et al.*, Neuropilin-1 is a host factor for SARS-CoV-2 infection. *Science* **370**, 861-865 (2020).
22. L. Cantuti-Castelvetri *et al.*, Neuropilin-1 facilitates SARS-CoV-2 cell entry and infectivity. *Science* **370**, 856-860 (2020).
23. J. Baggen *et al.*, Genome-wide CRISPR screening identifies TMEM106B as a proviral host factor for SARS-CoV-2. *Nat Genet*, (2021).
24. Z. Daniloski *et al.*, Identification of Required Host Factors for SARS-CoV-2 Infection in Human Cells. *Cell* **184**, 92-105 e116 (2021).
25. J. Wei *et al.*, Genome-wide CRISPR Screens Reveal Host Factors Critical for SARS-CoV-2 Infection. *Cell* **184**, 76-91 e13 (2021).
26. Y. Zhu *et al.*, A genome-wide CRISPR screen identifies host factors that regulate SARS-CoV-2 entry. *Nature communications* **12**, 961 (2021).
27. M. E. Dieterle *et al.*, A Replication-Competent Vesicular Stomatitis Virus for Studies of SARS-CoV-2 Spike-Mediated Cell Entry and Its Inhibition. *Cell Host Microbe* **28**, 486-496 e486 (2020).
28. S. Konermann *et al.*, Genome-scale transcriptional activation by an engineered CRISPR-Cas9 complex. *Nature* **517**, 583-588 (2015).

29. S. Zhu *et al.*, Guide RNAs with embedded barcodes boost CRISPR-pooled screens. *Genome Biol* **20**, 20 (2019).
30. M. A. Horlbeck *et al.*, Compact and highly active next-generation libraries for CRISPR-mediated gene repression and activation. *eLife* **5**, (2016).
31. D. Wrapp *et al.*, Cryo-EM structure of the 2019-nCoV spike in the prefusion conformation. *Science* **367**, 1260-1263 (2020).
32. Y. Zhou *et al.*, Metascape provides a biologist-oriented resource for the analysis of systems-level datasets. *Nature communications* **10**, 1523 (2019).
33. S. Ranganathan *et al.*, LRAD3, a novel low-density lipoprotein receptor family member that modulates amyloid precursor protein trafficking. *J Neurosci* **31**, 10836-10846 (2011).
34. M. Hiraizumi, K. Yamashita, T. Nishizawa, O. Nureki, Cryo-EM structures capture the transport cycle of the P4-ATPase flippase. *Science* **365**, 1149-1155 (2019).
35. T. Gramberg *et al.*, LSECtin interacts with filovirus glycoproteins and the spike protein of SARS coronavirus. *Virology* **340**, 224-236 (2005).
36. E. Karaca *et al.*, Genes that Affect Brain Structure and Function Identified by Rare Variant Analyses of Mendelian Neurologic Disease. *Neuron* **88**, 499-513 (2015).
37. D. R. Al-Sharaky *et al.*, ROC-1, P21 and CAIX as markers of tumor aggressiveness in bladder carcinoma in Egyptian patients. *Diagn Pathol* **15**, 33 (2020).
38. M. Fan *et al.*, New Gene Variants Associated with the Risk of Chronic HBV Infection. *Virol Sin* **35**, 378-387 (2020).
39. S. Matsuyama *et al.*, Enhanced isolation of SARS-CoV-2 by TMPRSS2-expressing cells. *Proc Natl Acad Sci U S A* **117**, 7001-7003 (2020).
40. M. Hoffmann, H. Kleine-Weber, S. Pohlmann, A Multibasic Cleavage Site in the Spike Protein of SARS-CoV-2 Is Essential for Infection of Human Lung Cells. *Mol Cell* **78**, 779-784 e775 (2020).
41. J. Buchrieser *et al.*, Syncytia formation by SARS-CoV-2-infected cells. *Embo J* **40**, e107405 (2021).
42. M. Uhlen *et al.*, Proteomics. Tissue-based map of the human proteome. *Science* **347**, 1260419 (2015).
43. H. Ma *et al.*, LDLRAD3 is a receptor for Venezuelan equine encephalitis virus. *Nature* **588**, 308-314 (2020).
44. A. Dominguez-Soto *et al.*, The pathogen receptor liver and lymph node sinusoidal endotelial cell C-type lectin is expressed in human Kupffer cells and regulated by PU.1. *Hepatology* **49**, 287-296 (2009).
45. M. McCallum *et al.*, N-terminal domain antigenic mapping reveals a site of vulnerability for SARS-CoV-2. *Cell*, (2021).
46. X. Chi *et al.*, A neutralizing human antibody binds to the N-terminal domain of the Spike protein of SARS-CoV-2. *Science* **369**, 650-655 (2020).
47. C. Engler, R. Gruetzner, R. Kandzia, S. Marillonnet, Golden gate shuffling: a one-pot DNA shuffling method based on type IIs restriction enzymes. *PLoS One* **4**, e5553 (2009).
48. Y. Liu *et al.*, Genome-wide screening for functional long noncoding RNAs in human cells by Cas9 targeting of splice sites. *Nat Biotechnol* **36**, 1203-1210 (2018).
49. R. Kolde, S. Laur, P. Adler, J. Vilo, Robust rank aggregation for gene list integration and meta-analysis. *Bioinformatics* **28**, 573-580 (2012).
50. S. Du *et al.*, Structurally Resolved SARS-CoV-2 Antibody Shows High Efficacy in Severely Infected Hamsters and Provides a Potent Cocktail Pairing Strategy. *Cell* **183**, 1013-1023 e1013 (2020).

Acknowledgements

We acknowledge the National Center for Protein Sciences (Beijing) at Peking University for their assistance with fluorescence-activated cell sorting, particularly Dr. J.L., Ms H. Y., and Ms L.D. for their technical help. We acknowledge Dr. Ying Yu (Peking University) for her assistance in preparing the NGS library. **Funding:** This project was supported by funds from National Key R&D Program of China 2020YFA0707800 to W.W., 2020YFA0707600 to Z.Z.; Beijing Municipal Science & Technology

Commission (Z181100001318009), the National Science Foundation of China (31930016), Beijing Advanced Innovation Center for Genomics at Peking University and the Peking-Tsinghua Center for Life Sciences (to W.W.); the National Science Foundation of China (31870893), the National Major Science & Technology Project for Control and Prevention of Major Infectious Diseases in China (2018ZX10301401, to Z.Z.); and China Postdoctoral Science Foundation (2020M670031, to Y.L.).

Author Contributions

W.W. conceived and supervised this project. W.W., S.Z., Y.L., and Z.Z. (Zhou) designed the experiments. S.Z. and Y.L. performed the CRISPRa screening and the following validations with the help from A.C., F.T., Y.X., C.W., Q.L., X.N., and Q.P.. X.X. performed the authentic SARS-CoV-2 virus infection with the help from X.D., under the supervision of J.W.. Z.Z. (Zhang) performed the protein purification and pull-down assay with the help from S.C. and S.D., under the supervision of J.X.. Z.L. performed the bioinformatics analysis. S.Z., Y.L., Z.Z. (Zhou), and W.W. wrote the manuscript with the help of all other authors.

Author Information The authors declare no competing financial interests. Readers are welcome to comment on the online version of the paper. Correspondence and requests for materials should be addressed to W.W. (wswei@pku.edu.cn), J.W. (wangjw28@163.com) and J.X. (junyuxiao@pku.edu.cn).